Theory of nanofibre excitation by a pulsed light beam

2007 J. Phys.: Condens. Matter 19 236220

(http://iopscience.iop.org/0953-8984/19/23/236220)

IOP PUBLISHING JOURNAL OF PHYSICS: CONDENSED MATTER

J. Phys.: Condens. Matter **19** (2007) 236220 (12pp) doi:10.1088/0953-8984/19/23/236220

Theory of nanofibre excitation by a pulsed light beam

V G Bordo[1]

Institut for Fysik og Kemi, Syddansk Universitet, DK-5230 Odense M, Denmark

E-mail: bordo@space.ru

Received 28 January 2007, in final form 25 April 2007
Published 15 May 2007
Online at stacks.iop.org/JPhysCM/19/236220

Abstract

The theory of scattering of a focused pulsed light beam from a dielectric nanofibre is developed. The nanofibre radius is assumed to be of the order of the light wavelength but much less than the beam radius. An analytical solution of the problem in terms of rapidly converging series of the Bessel and Hankel functions is derived. It is shown that the result can be described as excitation of the nanofibre transient normal modes for which the dispersion curves are obtained. These findings can be used for optimizing both the photoluminescence output and polarization, as well as the laser action of a nanofibre.

1. Introduction

Recent progress in the fabrication of submicron-sized structures has allowed one to grow optical fibres, both inorganic and organic, having transverse dimensions of the order of 100 nm. They have been given the name nanofibres or nanowires, and currently they can be grown from InP [1, 2], ZnO [3], GaN [4], CdS [5], different *p*-phenylene oligomers [6, 7] as well as functionalized *p*-phenylene molecules [8], and they can be fabricated from silica [9]. These structures demonstrate promising optical properties in photoluminescence, photodetection [2, 10] and waveguiding [9, 11–13] and can operate as an active medium for laser generation [3–5, 12, 14–16]. All these factors allow one to believe that nanofibres will find broad applications in future submicron optical and optoelectronic devices.

Although the electrodynamical problems for such structures can be solved numerically, by direct solving of Maxwell's equations, the underlying physics can be obscured in that approach. In contrast with that, an analytical solution, when available, significantly simplifies the analysis. The exact solution of the problem of diffraction of a plane electromagnetic wave at perpendicular incidence by a dielectric cylinder of infinite length was first given by Lord Rayleigh [17, 18]. Much later, that result was generalized to the case of oblique incidence [19]. In the following studies [20–23], it has been noticed that the field amplitudes

[1] Permanent address: A M Prokhorov General Physics Institute, Russian Academy of Sciences, 119991 Moscow, Russia.

at perpendicular incidence exhibit resonances at certain frequencies that have been used for a precise determination of fibre diameters as well as of their deviation from circularity [21, 24]. These resonances have been obtained numerically for very large values of the size parameter, $k_d a = 2\pi a/\lambda_d$ with a the cylinder radius and λ_d the wavelength in the dielectric, that does not allow the use of that analysis in other domains of $k_d a$.

Recently, we have obtained an exact analytical solution for the problem of light scattering from a dielectric semicylinder placed on an ideally reflecting plane [25]. This model system can be used for the description of scattering from nanofibres grown on a substrate. However in all the studies mentioned above the incident radiation was assumed to be a plane monochromatic electromagnetic wave, whereas in many experiments carried out with nanofibres one deals with focused pulsed laser beams. It is the aim of the present paper to bridge this gap in the theory. We consider two different models for a nanofibre: (i) a dielectric cylinder, and (ii) a dielectric semicylinder placed on an ideally reflecting plane. It should be noted that in the general case the problem of scattering of a focused beam by a cylinder is rather complicated [26]. In this paper, assuming that the nanofibre diameter is much less than the focus diameter and applying the two-dimensional Fourier transform we obtain the complete solution of the problem for oblique incidence in terms of rapidly converging series of the Bessel and Hankel functions. We analyse the nanofibre normal modes corresponding to the resonances in the field components and calculate their dispersion curves in the domain of small size parameters. Although the solution obtained describes the fields in both the nanofibre interior and exterior, we focus our attention on the electric field energy inside the nanofibre, which is directly related to its photoluminescence and laser action. We show that nanofibre excitation can be clearly described in terms of normal modes which are transient either along the nanofibre axis or in time.

The paper is organized as follows. In section 2.1 we present the basic equations which are necessary for further consideration. Section 2.2 is devoted to the discussion of the nanofibre normal modes and their dispersion curves. In section 2.3 we derive the expression for the electric field energy inside the nanofibre. In section 2.4 we extend the approach considered above to a semicylinder on an ideally reflecting surface. The results obtained are illustrated by some numerical calculations in section 3. In section 4 we summarize the main results of this work.

2. Theory

2.1. Basic equations

Let us assume that a nanofibre has a circular cross-section of radius a, the beam axis crosses the nanofibre axis, and the pulse shape and the beam profile are Gaussian. We choose the z axis along the nanofibre axis and the y axis in the plane containing both the z axis and the beam axis (see figure 1). Let both the nanofibre and surrounding medium be isotropic and be characterized by the dielectric functions ϵ_2 and ϵ_1, respectively. Then the incident wave electric field can be written as

$$\mathbf{E}^{\mathrm{i}}(x, y, z, t) = \mathbf{E}_0^{\mathrm{i}}(x, y, z, t) \exp(-\mathrm{i}q_1 y + \mathrm{i}\beta_0 z - \mathrm{i}\omega_0 t), \tag{1}$$

where the field amplitude is given by[2]

$$\mathbf{E}_0^{\mathrm{i}}(x, y, z, t) = \mathbf{E}_0 \exp\left[-\frac{x^2 + (y\sin\alpha + z\cos\alpha)^2}{2\sigma^2}\right] \exp\left(-\frac{t^2}{2\tau^2}\right) \tag{2}$$

[2] It is assumed here that the beam radius is much larger than the wavelength and the pulse duration is much longer than the period of the field oscillations so that the field of the form (1) approximately satisfies the wave equation.

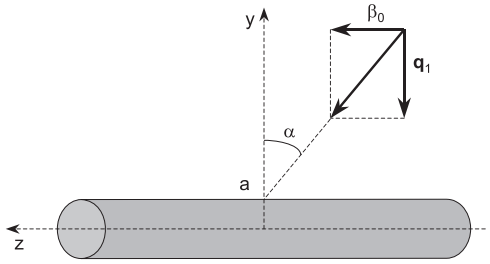

Figure 1. Geometry of the problem.

with $-q_1$ and β_0 the projections of the wave vector onto the axes y and z, respectively, ω_0 the frequency of the incident wave, α the angle of incidence with respect to the y axis, and σ and τ the radius and pulse duration of the light beam. A similar expression is valid for the magnetic field of the incident beam.

We shall consider the case where the beam radius is much larger than the nanofibre radius, $\sigma \gg a$. Then, in the vicinity of the nanofibre, (2) is reduced to the following one[3]:

$$\mathbf{E}_0^{\mathrm{i}}(z,t) \approx \mathbf{E}_0 \exp\left(-\frac{z^2\cos^2\alpha}{2\sigma^2}\right)\exp\left(-\frac{t^2}{2\tau^2}\right). \tag{3}$$

On the other hand, the beam radius will be assumed to be much less than the nanofibre length. In such a case one can neglect the edge effects and consider the nanofibre as infinitely long.

The total electric field can be written in the form

$$\mathbf{E} = \begin{cases} \mathbf{E}^{\mathrm{i}} + \mathbf{E}^{\mathrm{s}} & \text{if } r > a; \\ \mathbf{E}^{\mathrm{f}} & \text{if } r < a, \end{cases} \tag{4}$$

where $\mathbf{E}^{\mathrm{s}}$ and $\mathbf{E}^{\mathrm{f}}$ are the electric field vector of the scattered field and the field inside the nanofibre, respectively. A similar expression is valid for the magnetic field vector. The fields $\mathbf{E}^{\mathrm{s}}$ and $\mathbf{E}^{\mathrm{f}}$ can be found in terms of the z component of the Hertz vector, ψ, satisfying the scalar wave equation [27]. We shall seek ψ in the form of the Fourier integral

$$\psi(x,y,z,t) = \frac{1}{(2\pi)^2}\int_{-\infty}^{\infty}\int_{-\infty}^{\infty}\tilde{\psi}(x,y;\beta,\omega)\mathrm{e}^{\mathrm{i}\beta z-\mathrm{i}\omega t}\mathrm{d}\beta\,\mathrm{d}\omega, \tag{5}$$

where the Fourier-transformed quantity $\tilde{\psi}(x,y;\beta,\omega)$ can be represented as a sum of two contributions associated with TM (transverse magnetic) and TE (transverse electric) polarizations. The corresponding scalar functions are found as expansions

$$\tilde{\psi}^{\mathrm{TM}}(r,\theta;\beta,\omega) = \frac{1}{q_j^2}\sum_{n=0}^{\infty} Z_n(q_j r)[a_n(\beta,\omega)\sin(n\theta) + b_n(\beta,\omega)\cos(n\theta)] \tag{6}$$

and

$$\tilde{\psi}^{\mathrm{TE}}(r,\theta;\beta,\omega) = \frac{1}{q_j^2}\sum_{n=0}^{\infty} Z_n(q_j r)[c_n(\beta,\omega)\sin(n\theta) + d_n(\beta,\omega)\cos(n\theta)], \tag{7}$$

where the functions $Z_n(X)$ are determined as

$$Z_n(X) = \begin{cases} H_n^{(1)}(q_1 r) & \text{if } r > a; \\ J_n(q_2 r) & \text{if } r < a, \end{cases} \tag{8}$$

with

$$q_j = \sqrt{\frac{\omega_0^2}{c^2}\epsilon_j - \beta_0^2}, \tag{9}$$

[3] This approximation is valid outside the nanofibre region $|z| \leqslant a\tan\alpha$.

J_n and $H_n^{(1)}$ are Bessel functions of the first kind and Hankel functions, respectively, and we have introduced the polar coordinates (r, θ) in the xy plane. Here, the subscript j labels different media: $j = 1$ corresponds to the surrounding medium, whereas $j = 2$ denotes the nanofibre interior.

The continuity of the tangential components of the total fields, E_θ, E_z, H_θ, and H_z, across the boundary $r = a$ leads to the equations for the coefficients a_n^{f}, b_n^{f}, c_n^{f}, d_n^{f}, and a_n^{s}, b_n^{s}, c_n^{s}, d_n^{s}, where the superscripts f and s refer to the fields inside the fibre and outside it, respectively. Finally, one obtains the equations for the Fourier-transformed quantities which formally coincide with those derived for an incident plane monochromatic electromagnetic wave [25] if instead of its field one takes the Fourier transform of (1),

$$\tilde{\mathbf{E}}^{\mathrm{i}}(y; \beta, \omega) = \tilde{\mathbf{E}}_0^{\mathrm{i}}(\beta, \omega) \exp(-\mathrm{i}q_1 y) \tag{10}$$

with

$$\tilde{\mathbf{E}}_0^{\mathrm{i}}(\beta, \omega) = \mathbf{E}_0 \frac{2\pi\sigma\tau}{\cos\alpha} \exp\left[-\frac{(\beta - \beta_0)^2\sigma^2}{2\cos^2\alpha}\right] \exp\left[-\frac{(\omega - \omega_0)^2\tau^2}{2}\right]. \tag{11}$$

Then the Fourier-transformed electric field components in the nanofibre interior written in the cylindrical coordinates (r, θ, z) can be represented as

$$\tilde{E}_\mu(r, \theta; \beta, \omega) = \tilde{E}_0^{\mathrm{i}}(\beta, \omega) \sum_{n=0}^{\infty} \left[A_{\mu n}(r; \beta, \omega) \sin(n\theta) + B_{\mu n}(r; \beta, \omega) \cos(n\theta)\right], \tag{12}$$

where the subscript μ runs over the components r, θ, and z, and the functions $A_{\mu n}$ and $B_{\mu n}$ are given in the appendix. Analogous expressions can be found for the field components outside the nanofibre (see [25] for detail).

Taking the inverse Fourier transform of (12),

$$E_\mu(r, \theta, z, t) = \frac{1}{(2\pi)^2} \int_{-\infty}^{\infty} \int_{-\infty}^{\infty} \tilde{E}_\mu(r, \theta; \beta, \omega) \mathrm{e}^{\mathrm{i}\beta z - \mathrm{i}\omega t} \mathrm{d}\beta \, \mathrm{d}\omega, \tag{13}$$

one obtains the solution of the problem under consideration. The integrand in (13) has poles given by the zeros of the denominators $D_n(\beta, \omega)$ in (A.7)–(A.10). On the other hand, these zeros determine the allowed values of pairs (β, ω) for the electromagnetic field in a free nanofibre, i.e. its normal modes [27].

2.2. *Nanofibre normal modes*

Among the solutions of the equations

$$D_n(\beta, \omega) = 0, \tag{14}$$

there are those which are given by pairs of real quantities $(\beta_{nm}, \omega_{nm})$. They correspond to the waveguiding (bound) modes. Such modes provide a complete description of the light propagation along the fibre in the steady-state regime far from the light source [28]. Besides that, (14) has solutions for which either β or ω, or both have imaginary parts, i.e.,

$$\beta = \beta^r + \mathrm{i}\beta^{\mathrm{i}}, \tag{15}$$

$$\omega = \omega^r - \mathrm{i}\omega^{\mathrm{i}}. \tag{16}$$

The contribution of such poles to the integral (13) leads to the transients along the fibre length or in time, or in both length and time, respectively. If β^{i} is small, the modes of the first type can propagate over long distances and their portions localized within or near the fibre core are known as leaky modes [28]. In the following, we shall call the first-type modes *space-decaying* modes, and the second-type ones *time-decaying* modes.

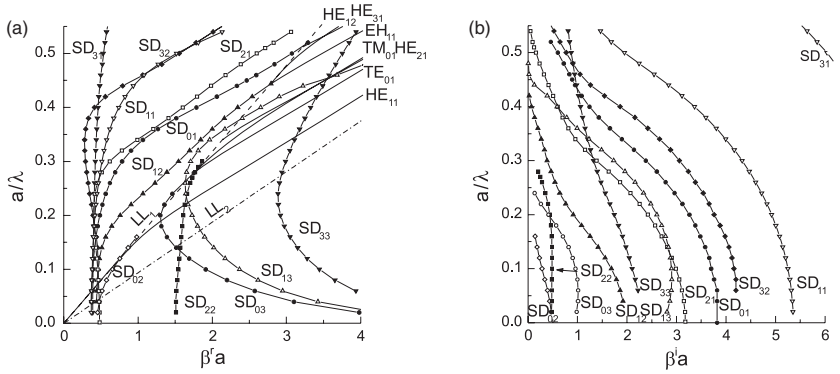

Figure 2. Dispersion curves of the SD modes: (a) for the real parts of the mode propagation constants; (b) for their imaginary parts. The modes with very large values of β^{i} are not shown in the figure. $\epsilon_1 = 1$, $\epsilon_2 = 2.89$.

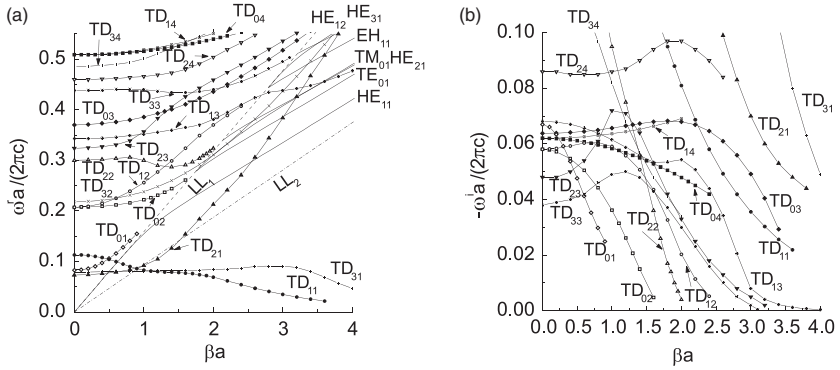

Figure 3. Dispersion curves of the TD modes: (a) for the real parts of the mode frequencies; (b) for their imaginary parts which fall into the range $|\omega^{\mathrm{i}}a/(2\pi c)| \leqslant 0.1$. $\epsilon_1 = 1$, $\epsilon_2 = 2.89$.

Figure 2(a) shows the dispersion curves $\omega(\beta^r)$ calculated numerically for the space-decaying modes, SD_{nm}, with $n = 0$–3 assuming $\epsilon_1 = 1$ and $\epsilon_2 = 2.89$ corresponding to an isotropic *para*-hexaphenyl film, and represented in dimensionless variables. The dispersion curves for the bound modes are also shown in this figure. They are disposed between the light lines $\omega = c\beta/\sqrt{\epsilon_1}$ (LL_1) and $\omega = c\beta/\sqrt{\epsilon_2}$ (LL_2), and are denoted as it is accepted in optical waveguide theory [28]. The dispersions for the imaginary parts of the zeros for the SD modes, $\omega(\beta^{\mathrm{i}})$, are shown in figure 2(b). Figure 3(a) represents the dispersion relations $\omega^r(\beta)$ for $n = 0$–3 calculated for the time-decaying modes, TD_{nm}. The dispersions of the corresponding imaginary parts, $\omega^{\mathrm{i}}(\beta)$, for the modes which are not strongly decaying are shown in figure 3(b). The subscript m enumerates the modes with a given n according to the order they approach the axis β^r for the SD modes or the axis ω^r for the TD modes. One can observe that some of these modes, both space- and time-decaying, can be considered as a continuation of waveguiding modes beyond the cutoff which coincides with the light line LL_1. The imaginary parts of the propagation constants or frequencies for such modes increase with the deviation of the corresponding real parts from the cutoff.

2.3. Calculation of the field inside the nanofibre

The integral (13) which determines the field components inside the nanofibre can be written in terms of the dimensionless parameters

$$\bar{\beta} = \beta a, \qquad \bar{\omega} = \frac{\omega}{c}a, \qquad \bar{z} = \frac{z}{a}, \qquad \bar{t} = \frac{ct}{a}. \tag{17}$$

When carrying out the integration, one can take into account that the function $\tilde{E}_0^{\mathrm{i}}(\bar{\beta}, \bar{\omega})$ in the integrand is essentially different from zero around its maximum at $\bar{\beta} = \bar{\beta}_0 \equiv \beta_0 a$ and $\bar{\omega} = \bar{\omega}_0 \equiv \omega_0 a/c$. The widths of the corresponding peak along the variables $\bar{\beta}$ and $\bar{\omega}$ are determined by the quantities

$$\Delta\bar{\beta} = \frac{\sqrt{2}a\cos\alpha}{\sigma} \tag{18}$$

and

$$\Delta\bar{\omega} = \frac{\sqrt{2}a}{c\tau}, \tag{19}$$

respectively. For typical experimental parameters, $a \leqslant 100$ nm, $\sigma \geqslant 2.5\ \mu$m, and $\tau \geqslant 100$ fs, one has $\Delta\bar{\beta} \leqslant 0.05$ and $\Delta\bar{\omega} \leqslant 0.005$ (correspondingly, $\Delta\bar{\omega}/(2\pi) \leqslant 0.0008$). On the other hand, the factors in front of the coefficients a_n^{f}, b_n^{f}, c_n^{f}, and d_n^{f} in (A.1)–(A.6), as well as the numerators in (A.7)–(A.10), vary significantly on the scales $\bar{\beta} \sim 1$ and $\bar{\omega} \sim 1$. The remaining factors, $D_n^{-1}(\bar{\beta}, \bar{\omega})$, vary most rapidly in the vicinity of the roots of (14), $(\bar{\beta}_{nm}, \bar{\omega}_{nm})$, and the scales of this variation along the variables $\bar{\beta}$ and $\bar{\omega}$ are determined by the quantities $\bar{\beta}_{nm}^{\mathrm{i}}$ and $\bar{\omega}_{nm}^{\mathrm{i}}$, respectively. Turning to figures 2 and 3, one can conclude that everywhere in the radiation region (i.e. to the left from the light line LL_1), except for a very narrow interval near the cutoff[4], one has $\bar{\beta}_{nm}^{\mathrm{i}} \gg \Delta\bar{\beta}$ and $\bar{\omega}_{nm}^{\mathrm{i}} \gg \Delta\bar{\omega}$. This means that in the case of non-grazing incidence, when performing the integration in (13) one can take the functions $A_{\mu n}(\beta, \omega)$ and $B_{\mu n}(\beta, \omega)$ off the integral at the point (β_0, ω_0). The remaining integration leads to the result

$$E_\mu(r, \theta, z, t) = E_0^{\mathrm{i}}(z, t)\exp(\mathrm{i}\beta_0 z - \mathrm{i}\omega_0 t) \times \sum_{n=0}^{\infty}\left[A_{\mu n}(r; \beta_0, \omega_0)\sin(n\theta) + B_{\mu n}(r; \beta_0, \omega_0)\cos(n\theta)\right], \tag{20}$$

where $E_0^{\mathrm{i}}(z, t)$ is the amplitude of the incident wave, (3). In other words, under typical experimental conditions the illumination by a pulsed light beam can be treated as the case of an incident plane monochromatic wave if instead of its amplitude, E_0, one substitutes the pulsed beam envelope function, $E_0^{\mathrm{i}}(z, t)$.

Using (20) one can calculate the distribution of the electric field energy in the nanofibre interior,

$$W(z, t) = \frac{\epsilon_2}{16\pi}\int_0^{2\pi}\mathrm{d}\theta\int_0^a\sum_\mu |E_\mu(r, \theta, z, t)|^2 r\,\mathrm{d}r. \tag{21}$$

This quantity is found as

$$W(z, t) = W_0\exp\left(-\frac{z^2\cos^2\alpha}{\sigma^2}\right)\exp\left(-\frac{t^2}{\tau^2}\right) \tag{22}$$

with

$$W_0 = \frac{\epsilon_2}{8}E_0^2\sum_{n=0}^{\infty}\left(\frac{3}{2} - \tau_n\right)\sum_\mu\int_0^a\left[(1-\delta_{n0})\left|A_{\mu n}(r; \beta_0, \omega_0)\right|^2 + \left|B_{\mu n}(r; \beta_0, \omega_0)\right|^2\right] r\,\mathrm{d}r, \tag{23}$$

where δ_{n0} is the Kronecker delta and τ_n is defined by (A.17).

[4] Note that in figures 2(b) and 3(b) the cutoff corresponds to the axes a/λ and βa, respectively.

If the frequency of the incident light, ω_0, falls into the nanofibre absorption band, the energy distribution given by (22), after some relaxation processes, leads eventually to photoluminescence from the nanofibre. If in experiment one varies either the angle of incidence of the light beam at a fixed frequency, or tunes the light frequency at a fixed angle of incidence, the photoluminescence output will also change. In the former case, the energy (22) has maxima at the values $\beta_0 = \beta^r_{nm}$ corresponding to the space-decaying modes. In the latter case, the maxima in energy occur at $\omega_0 = \omega^r_{nm}$ and correspond to the time-decaying modes. The widths of those peaks are determined by the quantities $\beta^{\rm i}_{nm}$ and $\omega^{\rm i}_{nm}$, respectively[5].

It is worthwhile to note that both SD and TD modes which correspond to the minima of the determinants D_n can manifest themselves also as resonances in the total intensity of light, $S_{\rm tot}$, scattered by the nanofibre [25]. As follows from the conservation of total electromagnetic energy, the maximum of the total field energy inside the nanofibre should correlate with the minimum of this quantity outside it. However, there is no such relation between the quantities W_0 and $S_{\rm tot}$ as the latter one is determined by the asymptotics of the scattered field in the far zone.

2.4. Semicylinder on an ideally reflecting surface

The approach developed above can be equally applied to the nanofibre model represented by a circular semicylinder placed on an ideally reflecting plane [25]. In such a case, one can use (20) with the following substitutions:

$$A_{\mu n} \to 2A_{\mu n}, \quad B_{\mu n} \to 0. \tag{24}$$

Then the sum over the modes which determines the quantity W_0 starts from $n = 1$, indicating that the modes with $n = 0$ are not excited in the nanofibre. The suppression of such modes is conditioned by the presence of the reflecting plane.

Let us consider the special case of normal incidence with respect to the substrate surface ($\alpha = 0$). In such a case the equations for TM and TE polarizations are completely separated [18]. This means that for TM incident wave polarization one can set in (7) $c_n = d_n = 0$. As a result, taking into account that $\beta_0 = 0$ one obtains the only non-zero coefficient A_{zn}. As it is seen from (6), this quantity dictates the $\sin(n\theta)$-dependence of the nth electric field mode. On the other hand, the incident wave electric field is determined by the factor

$$\mathrm{e}^{-\mathrm{i}q_1 r\sin\theta} = J_0(q_1 r) + 2\sum_{m=1}^{\infty} J_{2m}(q_1 r)\cos(2m\theta) - 2\mathrm{i}\sum_{m=1}^{\infty} J_{2m-1}(q_1 r)\sin[(2m-1)\theta]. \tag{25}$$

It follows from here that the incident wave can excite in the semicylinder only the modes with odd numbers n. An analogous consideration of TE incident wave polarization shows that both even and odd modes can be excited at normal incidence.

A similar selection rule occurs for the modes which are excited at normal incidence and can be observed in scattering. The total intensity scattered in all directions in the far zone per unit length of the nanofibre is found as follows [25]:

$$S_{\rm tot} = \frac{\omega}{2\pi q_1^2 r}\sum_{n=1}^{\infty}(\epsilon_1 \mid a_n^{\rm s} \mid^2 + \mid c_n^{\rm s} \mid^2), \tag{26}$$

where the coefficients $a_n^{\rm s}$ and $c_n^{\rm s}$ determine the $\sin(n\theta)$-dependence of the scalar functions $\tilde{\psi}^{\rm TM}$ and $\tilde{\psi}^{\rm TE}$, (6) and (7), in the surrounding medium. For TM polarization, $c_n^{\rm s} = 0$ and one obtains

[5] Besides the maxima relatively the light frequency discussed here, there may be also maxima originating from resonances in $\epsilon_2(\omega)$.

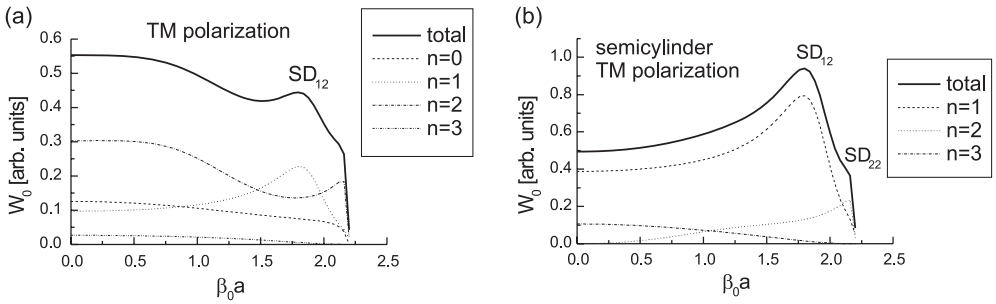

Figure 4. (a) W_0 as a function of β_0 calculated for $\epsilon_1 = 1$, $\epsilon_2 = 2.89$, and $\omega_0 a/(2\pi c) = 0.35$. TM incident wave polarization. (b) Same as (a) but for a semicylinder on an ideally reflecting surface.

the selection rule as above. For TE polarization, $a_n^{\mathrm{s}} = b_n^{\mathrm{s}} = 0$, whereas the component H_z^{i} in the incident wave has the θ-dependence given by (25). This means that, as in the case of TM polarization, only the modes with odd n can be observed in scattering.

3. Numerical results

Figure 4(a) shows the variation of W_0 with β_0 scanning the radiation region calculated for TM incident wave polarization with $\omega_0 a/(2\pi c) = 0.35$ and with an account of the terms $n = 0$–10 in (23). The energy drop at $\beta_0 a \approx 2.2$ originates from the approach to the cutoff at which $q_1 = 0$. The individual contributions from the terms with $n = 0$, 1, 2, and 3 are also shown in the figure, illustrating their rapid decrease with n. The curve corresponding to $n = 1$ exhibits a peak at $\beta_0 a \approx 1.8$ which is also seen in the total energy curve. Turning to figure 2(a) one can identify it as being originating from the mode SD_{12}. The contributions of the modes SD_{11} and SD_{13} are not pronounced because of the large values of β^{i} corresponding to them. A broader maximum to the left from the peak SD_{12} arises from the mode SD_{21}. The curve $n = 2$ also shows an increase corresponding to the mode SD_{22} just below the cutoff which is not pronounced in the total energy. For comparison, figure 4(b) illustrates the excitation of a semicylindrical nanofibre placed on an ideally reflecting surface. In such a case the zeroth term does not contribute to W_0 and the contribution of the term with $n = 2$ tends to zero with decreasing β_0 due to the selection rule considered in section 2.4. As a result, the peak corresponding to the SD_{12} mode becomes more distinct, and the mode SD_{22} manifests itself as a shoulder at the cutoff.

Another situation when the light beam frequency is varying at a fixed angle of incidence is illustrated in figure 5(a) for the case of a TM-polarized beam normally incident ($\alpha = 0$) on a cylindrical fibre. In this case the peaks in W_0 correspond to the time-decaying modes. Their origin can be deduced when comparing the positions of maxima which occur for different n with the mode frequencies at $\beta = 0$ in figure 3(a). In the case of a semicylinder placed on an ideally reflecting plane, only modes with odd n can be excited, due to the selection rule (figure 5(b)). These modes are also displayed in the spectrum of scattered light (figure 6). It should be noted that the modes distinct from those for TM polarization are pronounced in the energy spectrum when the nanofibre is excited by a normally incident TE-polarized light beam (not shown).

The data represented above allow one to calculate the excitation polarization ratio, ρ, defined as

$$\rho = \frac{W_0^{\mathrm{TM}} - W_0^{\mathrm{TE}}}{W_0^{\mathrm{TM}} + W_0^{\mathrm{TE}}}. \tag{27}$$

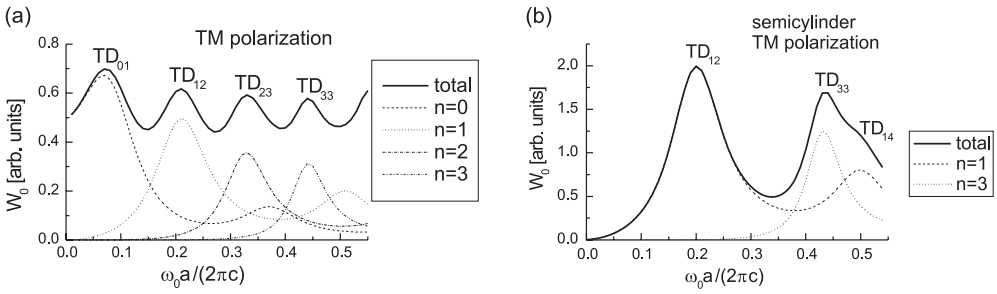

Figure 5. (a) W_0 as a function of ω_0 for normal incidence calculated for $\epsilon_1 = 1$, $\epsilon_2 = 2.89$. TM incident wave polarization. (b) Same as (a) but for a semicylinder on an ideally reflecting surface.

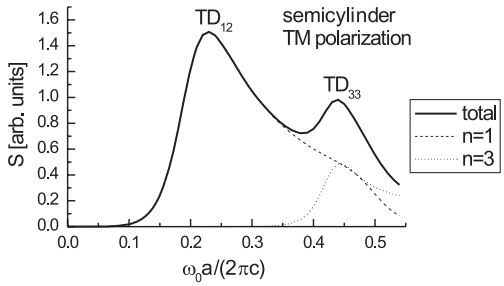

Figure 6. The intensity of light scattered in all directions in the far zone from a semicylinder placed on an ideally reflecting plane as a function of ω_0. Normal incidence, TM incident wave polarization. $\epsilon_1 = 1$, $\epsilon_2 = 2.89$.

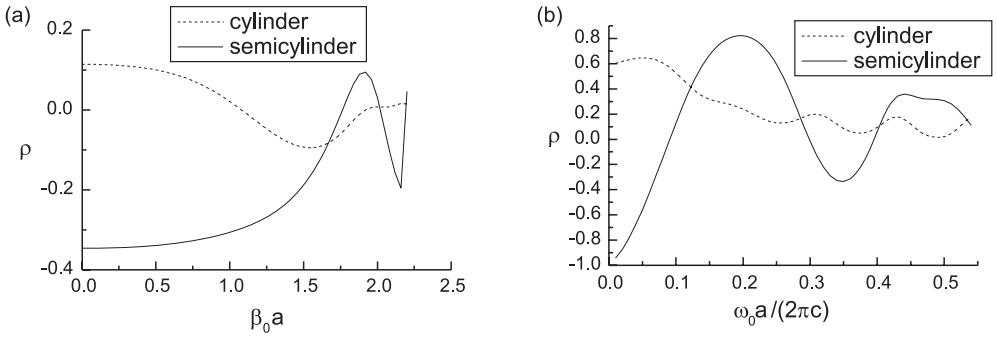

Figure 7. The excitation polarization ratio for a cylinder versus a semicylinder on an ideally reflecting surface: (a) as a function of β_0; (b) as a function of ω_0 at normal incidence. $\epsilon_1 = 1$, $\epsilon_2 = 2.89$.

The results obtained for the variation of either the angle of incidence or the beam frequency are shown in figures 7(a) and (b), respectively. One can see a dramatic change of both the polarization ratio values and its general behaviour introduced by the reflecting substrate. These remarkable variations of ρ display the mode structure of the electromagnetic field inside the nanofibre. A sharp peak in figure 7(a) is associated with the mode SD_{12}, whereas the pronounced maximum and minimum in figure 7(b) originate from different positions of the mode peaks in TM versus TE polarization.

It is interesting to note that the value of the polarization ratio at $\omega_0 = 0$, ρ_0, corresponds to the static limit and can be obtained as follows. The electric field amplitude inside the nanofibre

being in the external homogeneous electric field $\mathbf{E}_0$ is found as [29]

$$E_{\parallel} = E_0 \tag{28}$$

or

$$E_{\perp} = \frac{2\epsilon_1}{\epsilon_1 + \epsilon_2} E_0 \tag{29}$$

depending on whether the vector $\mathbf{E}_0$ is directed parallel or perpendicular to the fibre axis. Taking here $\epsilon_1 = 1$ and $\epsilon_2 = 2.89$, one gets the value $\rho_0 \approx 0.58$.

4. Conclusions

In this paper, we have developed the theory of scattering of a pulsed Gaussian light beam from a dielectric nanofibre. We have applied this theory to two models of a nanofibre. We have shown that both the electric field energy penetrated into the nanofibre and the intensity of the scattered light can be clearly described in terms of excitation of the nanofibre normal modes which, in contrast with the waveguiding modes, have either complex propagation constant or complex eigenfrequency. We have obtained the dispersion curves for these so-called space-decaying and time-decaying modes in the domain of small size parameters. This has helped us to interpret the dependence of the energy inside the nanofibre and of the integral scattered intensity on the beam incidence angle and frequency. It has been demonstrated that it is sufficient to calculate the first few terms in the field expansions to obtain an approximate solution. As a result, the mode structure of the fields contains only a few resonances. This situation differs remarkably from the calculations in the domain of large size parameters where the field distribution is much structured [22, 23].

The comparative analysis of the two models of a nanofibre has revealed that the ideally reflecting substrate suppresses the zeroth-order modes which correspond to an isotropic in the xy plane distribution of the electric field. Besides that, the presence of the reflecting plane introduces some selection rules at normal incidence. In the case of TM incident wave polarization, only odd modes can be excited inside the nanofibre. The same rule occurs for the integral intensity of the scattered light in the far zone for both TM and TE polarizations.

This study thus can be used for finding favourable conditions for energy input into the nanofibre, its photoluminescence efficiency and polarization.

Acknowledgments

The author is grateful to H-G Rubahn for hospitality during his stay at SDU. The financial support of this work from Forskningsrådet for Teknologi og Produktion (Denmark) is also gratefully acknowledged.

Appendix. Definition of the functions $A_{\mu n}$ and $B_{\mu n}$

The functions $A_{\mu n}$ and $B_{\mu n}$ which determine the Fourier transform of the electric field components in the nanofibre interior, (12), are defined as follows:

$$A_{rn}(r;\beta,\omega) = \frac{\mathrm{i}\beta}{q_2} J_n'(q_2 r) a_n^{\mathrm{f}}(\beta,\omega) - \frac{\mathrm{i}\omega n}{c q_2^2 r} J_n(q_2 r) d_n^{\mathrm{f}}(\beta,\omega), \tag{A.1}$$

$$B_{rn}(r;\beta,\omega) = \frac{\mathrm{i}\beta}{q_2} J_n'(q_2 r) b_n^{\mathrm{f}}(\beta,\omega) + \frac{\mathrm{i}\omega n}{c q_2^2 r} J_n(q_2 r) c_n^{\mathrm{f}}(\beta,\omega), \tag{A.2}$$

$$A_{\theta n}(r;\beta,\omega) = -\frac{\mathrm{i}\beta n}{q_2^2 r} J_n(q_2 r) b_n^{\mathrm{f}}(\beta,\omega) - \frac{\mathrm{i}\omega}{c q_2} J_n'(q_2 r) c_n^{\mathrm{f}}(\beta,\omega), \tag{A.3}$$

$$B_{\theta n}(r;\beta,\omega) = \frac{\mathrm{i}\beta n}{q_2^2 r} J_n(q_2 r) a_n^{\mathrm{f}}(\beta,\omega) - \frac{\mathrm{i}\omega}{c q_2} J_n'(q_2 r) d_n^{\mathrm{f}}(\beta,\omega), \tag{A.4}$$

$$A_{zn}(r;\beta,\omega) = J_n(q_2 r) a_n^{\mathrm{f}}(\beta,\omega), \tag{A.5}$$

$$B_{zn}(r;\beta,\omega) = J_n(q_2 r) b_n^{\mathrm{f}}(\beta,\omega). \tag{A.6}$$

Here, the prime above the Bessel function denotes differentiation with respect to its argument.

The coefficients a_n^{f}, b_n^{f}, c_n^{f}, and d_n^{f} have been introduced in (6) and (7). They are found from the boundary conditions for the field components at $r = a$ and have the form

$$a_n^{\mathrm{f}}(\beta,\omega) = \frac{D_{1n}(\beta,\omega)}{D_n(\beta,\omega)}, \tag{A.7}$$

$$b_n^{\mathrm{f}}(\beta,\omega) = -\frac{D_{2n}(\beta,\omega)}{D_n(\beta,\omega)}, \tag{A.8}$$

$$c_n^{\mathrm{f}}(\beta,\omega) = \frac{D_{3n}(\beta,\omega)}{D_n(\beta,\omega)}, \tag{A.9}$$

$$d_n^{\mathrm{f}}(\beta,\omega) = \frac{D_{4n}(\beta,\omega)}{D_n(\beta,\omega)}, \tag{A.10}$$

where D_n is the determinant of the matrix.

$$\hat{M}_n = \begin{pmatrix} J_n(q_2 a) & 0 & -H_n^{(1)}(q_1 a) & 0 \\ \frac{\mathrm{i}\beta n}{q_2^2 a} J_n(q_2 a) & -\frac{\mathrm{i}\omega}{c q_2} J_n'(q_2 a) & -\frac{\mathrm{i}\beta n}{q_1^2 a} H_n^{(1)}(q_1 a) & \frac{\mathrm{i}\omega}{c q_1} H_n^{(1)\prime}(q_1 a) \\ \frac{\mathrm{i}k_2^2 c}{\omega q_2} J_n'(q_2 a) & -\frac{\mathrm{i}\beta n}{q_2^2 a} J_n(q_2 a) & -\frac{\mathrm{i}k_1^2 c}{\omega q_1} H_n^{(1)\prime}(q_1 a) & \frac{\mathrm{i}\beta n}{q_1^2 a} H_n^{(1)}(q_1 a) \\ 0 & J_n(q_2 a) & 0 & -H_n^{(1)}(q_1 a) \end{pmatrix}. \tag{A.11}$$

In the case of TM polarization, D_{1n} and D_{4n} are the determinants of the matrices obtained from $\hat{M}_n$ by replacing the first and second columns with the column

$$\vec{F}_{1n}^{\mathrm{TM}} = \begin{pmatrix} -2\mathrm{i}\sigma_n \cos\alpha J_n(q_1 a) \\ 2\sigma_n \sin\alpha [n J_n(q_1 a)/q_1 a] \\ 2\sigma_n \sqrt{\epsilon_1} J_n'(q_1 a) \\ 0 \end{pmatrix} \tag{A.12}$$

respectively, and D_{2n} and D_{3n} are the determinants of the matrices obtained from $\hat{M}_n$ by replacing the first and second columns with the column

$$\vec{F}_{2n}^{\mathrm{TM}} = \begin{pmatrix} -2\tau_n(1-\sigma_n)\cos\alpha J_n(q_1 a) \\ -2\mathrm{i}\tau_n(1-\sigma_n)\sin\alpha [n J_n(q_1 a)/q_1 a] \\ -2\mathrm{i}\tau_n(1-\sigma_n)\sqrt{\epsilon_1} J_n'(q_1 a) \\ 0 \end{pmatrix}, \tag{A.13}$$

respectively. In the case of TE polarization, it is necessary to use, instead of (A.12) and (A.13)[6],

$$\vec{F}_{1n}^{\mathrm{TE}} = \begin{pmatrix} 0 \\ -2\mathrm{i}\tau_n(1-\sigma_n) J_n'(q_1 a) \\ -2\mathrm{i}\tau_n(1-\sigma_n)\sqrt{\epsilon_1}\sin\alpha [n J_n(q_1 a)/q_1 a] \\ 2\tau_n(1-\sigma_n)\sqrt{\epsilon_1}\cos\alpha J_n(q_1 a) \end{pmatrix}, \tag{A.14}$$

and

$$\vec{F}_{2n}^{\mathrm{TE}} = \begin{pmatrix} 0 \\ -2\sigma_n J_n'(q_1 a) \\ -2\sigma_n\sqrt{\epsilon_1}\sin\alpha [n J_n(q_1 a)/q_1 a] \\ -2\mathrm{i}\sigma_n\sqrt{\epsilon_1}\cos\alpha J_n(q_1 a) \end{pmatrix}, \tag{A.15}$$

[6] In [25], the vectors $\vec{F}_{1n}^{\mathrm{TE}}$ and $\vec{F}_{2n}^{\mathrm{TE}}$ were interchanged by mistake.

respectively. Besides that, we have introduced the following notations:

$$\sigma_n = \begin{cases} 0 & \text{if } n \text{ is even;} \\ 1 & \text{if } n \text{ is odd,} \end{cases} \tag{A.16}$$

and

$$\tau_n = \begin{cases} 1/2 & \text{if } n = 0; \\ 1 & \text{if } n \neq 0. \end{cases} \tag{A.17}$$

Similar equations can be written for the functions $A^{s}_{\mu n}$ and $B^{s}_{\mu n}$ which determine the field amplitudes outside the nanofibre. The corresponding expressions involve the Hankel functions $H^{(1)}(q_1 r)$ instead of the Bessel functions (see [25] for details).

References

[1] Duan X, Huang Y, Cui Y, Wang J and Lieber C M 2001 *Nature* **409** 66
[2] Wang J, Gudiksen M S, Duan X, Cui Y and Lieber C M 2001 *Science* **293** 1455
[3] Huang M H, Mao S, Feick H, Yan H, Wu Y, Kind H, Weber E, Russo R and Yang P 2001 *Science* **292** 1897
[4] Johnson J C, Choi H-J, Knutsen K P, Schaller R D, Yang P and Saykally R J 2002 *Nat. Mater.* **1** 106
[5] Duan X, Huang Y, Agarwal R and Lieber C M 2003 *Nature* **421** 241
[6] Balzer F and Rubahn H-G 2005 *Adv. Funct. Mater.* **15** 17
[7] Balzer F and Rubahn H-G 2001 *Appl. Phys. Lett.* **79** 3860
[8] Schiek M, Lützen A, Koch R, Al-Shamery K, Balzer F, Frese R and Rubahn H-G 2005 *Appl. Phys. Lett.* **86** 153107
[9] Tong L, Gattass R R, Ashcom J B, He S, Lou J, Shen M, Maxwell I and Mazur E 2003 *Nature* **426** 816
[10] Thilsing-Hansen K, Neves-Petersen M T, Petersen S B, Neuendorf R, Al-Shamery K and Rubahn H-G 2005 *Phys. Rev.* B **72** 115213
[11] Balzer F, Bordo V G, Simonsen A C and Rubahn H-G 2003 *Phys. Rev.* B **67** 115408
[12] Johnson J C, Yan H, Yang P and Saykally R J 2003 *J. Phys. Chem.* **107** 8816
[13] Barrelet C J, Greytak A B and Lieber C M 2004 *Nano Lett.* **4** 1981
[14] Agarwal R, Barrelet C J and Lieber C M 2005 *Nano Lett.* **5** 917
[15] Quochi F, Cordella F, Mura A, Bongiovanni G, Balzer F and Rubahn H-G 2005 *J. Phys. Chem.* **109** 21690
[16] Quochi F, Cordella F, Mura A, Bongiovanni G, Balzer F and Rubahn H-G 2006 *Appl. Phys. Lett.* **88** 041106
[17] Lord Rayleigh (Strutt J W) 1881 *Phil. Mag.* **12** 81
[18] van de Hulst H C 1957 *Light Scattering by Small Particles* (New York: Wiley) p 300
[19] Wait J R 1955 *Can. J. Phys.* **33** 189
[20] Van Bladel J 1977 *IEE J. Microw. Opt. Acoust. (GB)* **1** 41
[21] Owen J F, Barber P W, Messinger B J and Chang R K 1981 *Opt. Lett.* **6** 272
[22] Owen J F, Chang R K and Barber P W 1981 *Opt. Lett.* **6** 540
[23] Abushagur M A G and George N 1985 *Appl. Opt.* **24** 4141
[24] Ashkin A, Dziedzic J M and Stolen R H 1981 *Appl. Opt.* **20** 2299
[25] Bordo V G 2006 *Phys. Rev.* B **73** 205117
[26] See Lock J A 1997 *J. Opt. Soc. Am.* A **14** 640 and references therein
[27] Stratton J A 1941 *Electromagnetic Theory* (New York: McGraw-Hill)
[28] Snyder A W and Love J D 1983 *Optical Waveguide Theory* (London: Chapman and Hall)
[29] Landau L D, Lifshitz E M and Pitaevskii L P 1984 *Electrodynamics of Continuous Media* (Oxford: Pergamon)